

Global phase diagram for binary alloys with one magnetic component

V. Talanquer and C. Varea

Facultad de Química, Universidad Nacional Autónoma de México, 04510 México, Distrito Federal, México

A. Robledo

*Instituto de Física, Universidad Nacional Autónoma de México,
Apartado Postal 20-364, 01000 México, Distrito Federal, México*

(Received 27 June 1988)

We describe the global mean-field phase diagram for a binary alloy that contains one magnetic component. We obtain 12 types of system phase diagrams, each of which displays a different interaction of chemical (segregation or ordering) and magnetic (ferromagnetic or antiferromagnetic) long-range order. Our results follow from the known features of the phase diagrams along the symmetric sections of Griffiths's three-component (spin-1) model when both uniform and sublattice ordered states are considered. The multiple-phase coexistence and associated multicritical states of the spin-1 model appear in alloy language linked to previously unknown features such as first-order magnetic to paramagnetic transitions within chemically ordered phases, phase segregation among two magnetically ordered states, and first-order field-induced transitions.

I. INTRODUCTION

Because different types of long-range order can arise in a given material as temperature is lowered, a competition between two or more phase transitions often takes place over the physical ranges of the relevant thermodynamic variables. The resulting phase diagram varies from system to system, as this is determined by the relative strengths of the interactions involved. A representative example that has received some attention¹⁻³ is that of the interplay between chemical and magnetic long-range order in alloys that contain one or more magnetic components. The simplest situation, that of a binary alloy with one magnetic component offers the possibility of a systematic study because it can be modeled as a spin-1 Ising system. This model has been studied extensively⁴ and its (mean-field) global phase diagram for uniform phases has been known for some time.⁴ The extension of the diagram that considers sublattice-ordered phases is described in the preceding paper,⁵ referred to here as I. Here we translate the results of I to the language of the binary alloy and offer, we believe for the first time, a complete thermodynamic characterization for this type of system. That is, one that describes the detailed evolution from segregation to ordering of the species and from ferromagnetic to antiferromagnetic behavior.

The interaction energy parameter space of the model binary alloy with one magnetic component, represented by the heat of mixing and the magnetic coupling constant, appears divided into 12 zones of different phase behavior. These correspond to the 12 zones of different topological behavior into which the symmetric sections of the Furman, Dattagupta, and Griffiths's (FDG) energy triangles appear divided.⁵ (We make frequent use here of the terminology and notation employed and explained in I.) The symmetric section of the principal, or *P*, triangle

with energy parameters $a=b>0$ and $c>0$ yields the properties of segregating-ferromagnetic alloys. The types of multiple-phase coexistence among uniform phases characteristic of this triangle generate phase behavior that has been overlooked in the literature of magnetic alloys.^{1,2} Thus, four-phase coexistence associated with the "shield" region implies coexistence between two different paramagnetic phases and a ferromagnetic phase. On the other hand, four-phase coexistence associated with the corner of the *P* triangle becomes a line of first-order transitions between ferromagnetic phases of different magnetic component content. The multicritical points *D*, *CA*, *B*², etc. (the notation of which is explained in I), located on this symmetrical section bound the thermodynamic space regions where this behavior occurs. The symmetrical section of the *R* triangle with energy parameters $a=b<0$ and $c>0$ generates the phase diagrams for ordering-ferromagnetic alloys. The triple points of the type (*AA*)³ among sublattice-ordered phases characteristic of this triangle (see I) appear in magnetic language as phase coexistence between an ordered paramagnetic with an ordered ferromagnetic phase. The sixth-order multicritical point (*F*) on this triangle occurs when the above referred to first-order line terminates at the point where second-order ferromagnetic transitions for uniform phases originate.

The transformation described in I between the phase diagrams (at equal chemical potential differences) of pairs of energy points along symmetrical sections acquires a precise meaning in the language of the magnetic alloy. It transforms ferromagnetic into antiferromagnetic properties while it preserves the segregating or ordering quality of the system. Thus,⁵ the *P* symmetrical section maps into the symmetrical section of the *Q* triangle with $a=b>0$ and $c<0$ plus a portion of the symmetrical section of the opposite *S* triangle (that with $0>a=b>-\frac{1}{4}$

and $-1 < c < -\frac{1}{2}$). The remaining portion of the S section is given under this transformation by the full symmetrical section of the R triangle. In the presence of an applied magnetic field H , the interrelation between ferromagnetic and antiferromagnetic properties is broken. An applied field breaks the twofold degeneracy (spin-up, spin-down) of ferromagnetism and the fourfold degeneracy of chemically ordered antiferromagnetic states. Therefore, the properties of ferromagnetic and antiferromagnetic alloys evolve differently as H becomes different from zero. The global phase diagram of the FDG three-component model described in I provides, as would be expected, this evolution in a natural way.

The structure of the rest of the paper is as follows: the definition and the mean-field expressions for the model magnetic alloy are provided in the next section, together with a classification of the energy parameter space. In Sec. III we extend the outline of the previously mentioned global behavior. There we show representative phase diagrams in the mixed space of temperature T , magnetic field intensity H , and chemical composition x , since these are the experimentally accessible fields and density. Our main results are summarized in Sec. IV. We make use throughout the paper of the notation for phase coexistence and critical points introduced and explained in I.

II. BINARY ALLOY WITH ONE MAGNETIC COMPONENT

Consider a binary alloy with N_A atoms of a magnetic component A and N_B atoms of a nonmagnetic diluent species B on a regular lattice of $N = N_A + N_B$ sites. The magnetic component is given two spin directions $(+, -)$ as in a spin- $\frac{1}{2}$ Ising model. We consider a subdivision into two equivalent interpenetrating sublattices (α and β) such that the first neighbor pair of sites belong to different sublattices. Such a subdivision is naturally introduced in the simple-cubic and in the body-centered-cubic lattices. The probability of finding an atom A with its spin pointing up (down) on a site on sublattice i ($i = \alpha, \beta$) is denoted by n_{Ai}^+ (n_{Ai}^-), while that of finding an atom of type B there is n_{Bi} . We have $n_{Bi} = 1 - n_{Ai}^+ - n_{Ai}^-$. The sublattice i occupancy by atoms of type A is $n_{Ai} = n_{Ai}^+ + n_{Ai}^-$ and the composition of the alloy is $x = \frac{1}{2}(n_{A\alpha} + n_{A\beta})$.

In mean-field approximation, the grand potential per site ω of the model alloy with interactions restricted to nearest-neighbor pairs at temperature kT (with k Boltzmann's constant), chemical potential difference $\mu_A - \mu_B$, and external magnetic field H is given by

$$2\omega = kT \left[\sum_{i=\alpha,\beta} n_{Ai}^+ \ln(n_{Ai}^+) + n_{Ai}^- \ln(n_{Ai}^-) + n_{Bi} \ln(n_{Bi}) \right] + a(n_{A\alpha}^+ n_{B\beta} + n_{A\alpha}^- n_{B\beta} + n_{A\beta}^+ n_{B\alpha} + n_{A\beta}^- n_{B\alpha}) + c(n_{A\alpha}^+ n_{A\beta}^- + n_{A\beta}^+ n_{A\alpha}^-) - \sum_{i=\alpha,\beta} (\mu_A - \mu_B) n_{Ai} - \sum_{i=\alpha,\beta} H(n_{Ai}^+ - n_{Ai}^-). \quad (1)$$

Because B atoms are nonmagnetic, their interaction energy with nearest-neighbor atoms of kind A , denoted by a/q where q is the coordination number, does not distinguish between the two spin orientations of A . Interaction energies between nearest-neighbor atoms A , denoted by c/q , include both chemical and magnetic terms.

Comparing Eq. (1) with Eqs. (10) and (11) of I together with the identifications

$$x^\alpha = n_{A\alpha}^+, \quad y^\alpha = n_{A\alpha}^-, \quad z^\alpha = n_{B\alpha}, \quad (2a)$$

$$x^\beta = n_{A\beta}^+, \quad y^\beta = n_{A\beta}^-, \quad z^\beta = n_{B\beta}, \quad (2b)$$

$$v_1 = \mu_A - \mu_B + H, \quad v_2 = \mu_A - \mu_B - H, \quad (2c)$$

and

$$a = b \quad (2d)$$

leads to the thermodynamic potential equivalence

$$\omega = \frac{1}{2} v_1 (x^\alpha + x^\beta) - \frac{1}{2} v_2 (y^\alpha + y^\beta). \quad (3)$$

Also, minimization of ω in Eq. (1) with respect to n_{Ai}^+ and n_{Ai}^- leads to the same Euler-Lagrange equations that we solved numerically in I. Therefore, the system phase diagrams along the symmetrical sections $a = b$ of the FDG three-component model, when translated according to Eqs. (2a)–(2d), become those of the model magnetic alloy.

The discussion of the relationships between chemical and magnetic long-range order in the model alloy is facilitated by the consideration of the sublattice magnetizations $\xi_{Ai} = (n_{Ai}^+ - n_{Ai}^-)/n_{Ai}$, ($i = \alpha, \beta$), in terms of which the grand potential ω takes the form

$$2\omega = kT \left[\sum_{i=\alpha,\beta} n_{Ai} \ln n_{Ai} + (1 - n_{Ai}) \ln(1 - n_{Ai}) \right] - (4a - c) n_{A\alpha} n_{A\beta} - (\mu_A - \mu_B) (n_{A\alpha} + n_{A\beta}) + \frac{1}{2} kT \left[\sum_{i=\alpha,\beta} n_{Ai} [(1 + \xi_{Ai}) \ln(1 + \xi_{Ai}) + (1 - \xi_{Ai}) \ln(1 - \xi_{Ai})] \right] - \frac{1}{2} c n_{A\alpha} n_{A\beta} \xi_{A\alpha} \xi_{A\beta} - H (n_{A\alpha} \xi_{A\alpha} + n_{A\beta} \xi_{A\beta}). \quad (4)$$

The first three terms in Eq. (4) describe a simple binary alloy with heat of mixing $\Lambda = 4a - c$, while the last three terms represent the magnetic properties of species A . The magnetic coupling is given by the FDG parameter c weighted by the sublattice occupancies of A .

In the absence of external field H , the grand potential ω exhibits a special symmetry between ferromagnetic and antiferromagnetic behavior. To see this, consider two different alloys with interaction parameters (Λ, c) and (Λ', c') and stable states with densities $(n_{A\omega}, n_{B\omega}; \xi_{A\omega}, \xi_{B\omega})$ and $(n'_{A\omega}, n'_{B\omega}; \xi'_{A\omega}, \xi'_{B\omega})$. The identifications $T' = T$, $\Lambda' = \Lambda$, $c' = -c$, $n'_{A\omega} = n_{A\omega}$, $n'_{B\omega} = n_{B\omega}$, $\xi'_{A\omega} = \xi_{A\omega}$, and $\xi'_{B\omega} = -\xi_{B\omega}$ imply $\omega' = \omega$ and establish a relationship between ferromagnetic $\xi_{A\omega} > 0$ and $\xi_{B\omega} > 0$ and antiferromagnetic $\xi'_{A\omega} > 0$ and $\xi'_{B\omega} < 0$ states in the primed and unprimed alloy systems. This relationship relates the FDG energy parameters of the two systems according to $c' = -c$ and $a' = (2a - c)/2$. This is the mapping described in I for the symmetrical sections of the energy triangles and it is shown in Fig. 1 together with the 12 regions of different behavior found for the model alloy. The numbering shown there indicates the order in which we describe each type of system in Sec. III.

A preliminary analysis of the phase behavior of binary alloys with one magnetic species can be carried out through the superposition of "purely" chemical phase transformation lines on the "purely" magnetic ones. The first are constructed on the assumption of a background paramagnetic state ($\xi_{A_i} = 0$), while the second presuppose complete uniform mixing of the two components ($n_{A\alpha} = n_{B\beta} = x$). When $\Lambda > 0$, a segregation coexistence line $T_S(x)$ is bounded by an ordinary critical point with temperature $T_{sc} = \frac{1}{8}(4a - c)$ and composition $x_{sc} = \frac{1}{2}$. When $\Lambda < 0$, a second-order chemical ordering transition is given by $T_0 = \frac{1}{2}(-4a + c)x(1 - x)$. The purely magnetic transitions are described by the line $T_M = \frac{1}{2}|c|x$.

In Fig. 2 we show the superposition of the transition lines described above on a (T, x) diagram for ferromagnetic alloys. Figures 2(a)–2(c) correspond to the case $a > 0$ and $c > 0$, while in Fig. 2(d) $a < 0$ and $c > 0$. In Fig. 2(a), when c is small there is a portion of the coexistence line for segregation with temperatures above T_M . These transition temperatures T_S for the segregation of paramagnetic phases remain unchanged when magnetic interactions are taken into account. Similarly, the second-order magnetic transitions with $T_M > T_S$ do not change when chemical interactions are considered. The remaining portions of the T_M and T_S lines would experience change when all interactions are considered simultaneously. They may appear shifted to different temperatures or even become replaced by transitions of different nature. Segregation with $T_S < T_M$ would involve, of course, at least one ferromagnetic phase. As c is increased in value the portion of the coexistence curve T_S that falls above the line T_M becomes smaller, and the temperature range for segregation of two paramagnetic phases is reduced accordingly. Figure 2(b) shows the case when $c = \frac{2}{3}$ where the point $T_S = T_M$ at $x_{sc} = \frac{1}{2}$ is a tricritical point. According to Fig. 2(b) for this and larger values of c segregation is always between paramagnetic and ferromagnetic phases. When c reaches the value of $\frac{2}{3}$, T_{sc} vanishes and our simple construction only predicts ferromagnetic transformations. For $\frac{2}{3} < c < 1$ when the system has already acquired a negative heat of mixing, the situation remains the same since the chemical ordering curve T_0 always falls below T_M and it is only tangent to T_M when $c = 1$. This situation is shown in Fig. 2(c) where all chemically ordered states appear metastable with respect to uniform ferromagnetic states. In Fig. 2(d) we show the case when $a < 0$ and $c > 0$, that is, when the FDG energy point in I is in the R triangle. There, four different regions can be distinguished: uniform paramagnetic (UP),

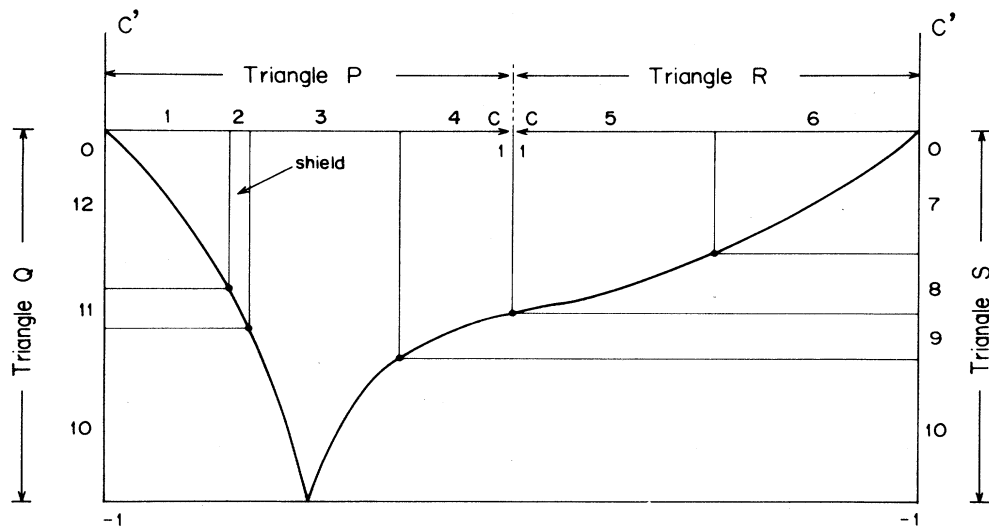


FIG. 1. The mapping for energy points on the symmetrical sections of the FDG energy triangles that relates the properties of ferromagnetic ($c > 0$) alloys to those of antiferromagnetic ($c < 0$) alloys in the absence of applied field.

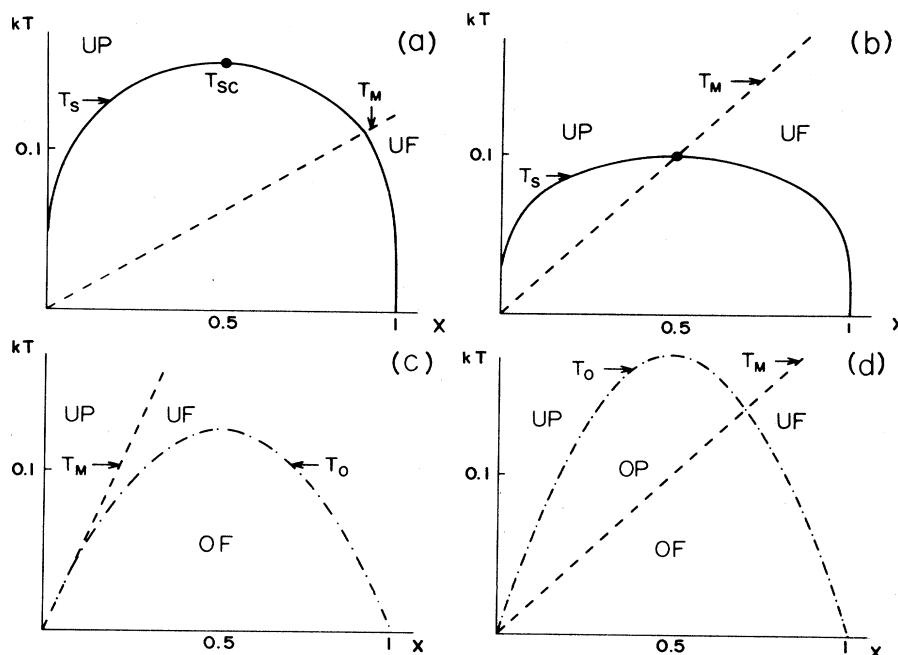


FIG. 2. Superposition of purely chemical and purely magnetic transitions in the space of temperature and composition. In (a) and (b) solid lines correspond to phase separation, and in (c) and (d) dashed-dotted lines represent second-order chemical ordering. Dashed lines indicate second-order magnetic transitions. In this and the rest of the figures KT is in units of the interaction parameter $|2a| + |c|$ which has been normalized to one throughout this work.

romagnetic (UF), ordered paramagnetic (OP), and ordered ferromagnetic (OF).

As we shall see in the next section, the exact mean-field phase diagrams differ considerably from those in Figs. 2(b)–2(d). Nevertheless, this simple construction, together with its antiferromagnetic equivalent, is a useful guideline in the interpretation of results.

III. SYSTEM PHASE DIAGRAMS

A few words about notation and the symmetry properties of the model in the absence of external field might be helpful before presenting details of the phase diagrams. When $H=0$, the grand potential ω is invariant under the transformation $\xi_{Ai} = -\xi_{Ai}$ and therefore every uniform ferromagnetic (UF) state corresponds to the coexistence of two states of opposite magnetization, namely A^2 in the notation of I. Equilibrium between two uniform paramagnetic (UP) states would also be denoted by A^2 . Critical points between two such UP states and second-order transitions between UP and UF phases are both denoted by B . The potential ω is also invariant with respect to interchange of sublattice indexes, and therefore chemically ordered paramagnetic (OP) and uniform antiferromagnetic (UA) states, both denoted by (AA) , are also double states. Ordered antiferromagnetic (OA) states are fourfold degenerate and correspond to coexistence of two sublattice-ordered states, namely $(AA)^2$ in the notation of I. At high temperatures $(AA)^2$ states terminate at critical points (BB) that represent OA to UA second-order transitions. The model predicts phase coex-

istence between OA and OP states, these correspond to the $(AA)^3$ -type states in I. These and other examples of phase coexistence and criticality are found on the symmetrical sections of the energy triangles. The temperature and energy parameter c location of the highest-order critical points and phase coexistence encountered along these sections⁵ is shown in Fig. 3. In this figure, features that are equivalent under the mapping described in the previous section appear at different temperatures. This is because here, as in I, we adopt the normalization condition $2|a| + |c| = 1$ for the energy parameters. See Eq. (21) of I.

A. Phase separation in ferromagnetic alloys ($a > 0, c > 0$)

The system phase diagrams for the symmetrical section of the principal energy triangle P have been discussed in detail by FDG.⁴ This section is divided into four regions of distinct phase behavior. In Fig. 3 they appear bounded by the values of c at which the multicritical points CA , BA^2 , and D occur. For values of c in the interval $0 < c < 0.294$ ($2 > \Lambda > 1.208$), magnetic interactions are weak and a representative phase diagram for this region, shown in Fig. 4(a) for $H=0$, has the same structure as that shown in Fig. 2(a). The position of the critical point B for chemically induced phase segregation is independent of the magnetic interactions in this range. The UP to UF transition is a straight line. The magnetic transition is present only at zero field, and phase segregation gradually shrinks towards zero temperature as H is increased. This simple behavior is shown in Figs. 4(b) and 4(c).

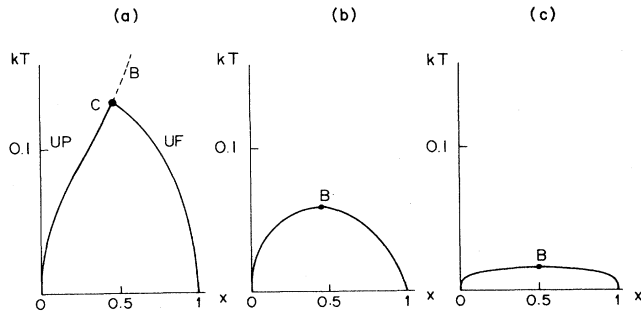


FIG. 6. System phase diagrams for a segregating-ferromagnetic alloy of region 3 in Fig. 1. (a)–(c) as in Fig. 4.

tions in this region of energy space. The results obtained from the transcription of the FDG diagrams for the R triangle differ from those previously mentioned in that there always occur first-order transitions between OP and OF states at low temperature. As shown in Fig. 3 the R -symmetrical section displays two distinct regions of phase behavior. In one region, with $1 > c > \frac{1}{2}$, $A^2(AA)$ states occur within a finite range of temperatures and are bounded by $(B)^2(AA)$ and (D) points at low and high temperature, respectively. In the other region, with $\frac{1}{2} > c > 0$, a similar situation occurs but with $(AA)^2$ states bounded by (CC) and $((D))$ points. These bounds for fourfold degenerate states meet at the sixth-order multicritical point (F) when $c = \frac{1}{2}$.⁵

In the region $1 > c > \frac{1}{2}$, ferromagnetic interactions are sufficiently strong for both the OP to UF and OP to OF phase transformations to be of the first order. The second-order transition lines from UP to OP and UP to UF states denoted in Fig. 8(a) by (B) and B , respectively, coincide with those of the superposition construction of Sec. II. The first-order OP–UF transitions, four-phase $A^2(AA)$ equilibrium when $H = 0$, meet the second-order UP–OP and UP–UF lines at a fourth-order critical point of type (D) . At low temperature, a small region of OF [or $(AA)^2$] states is found, and transformation of these states into UF or OP states are always of the second-order $(BB)^2$ and first-order $(AA)^3$ types when $H = 0$, respectively. The region of OF states terminates at a critical end point of type $(AA)(B)^2$. When a magnetic field is

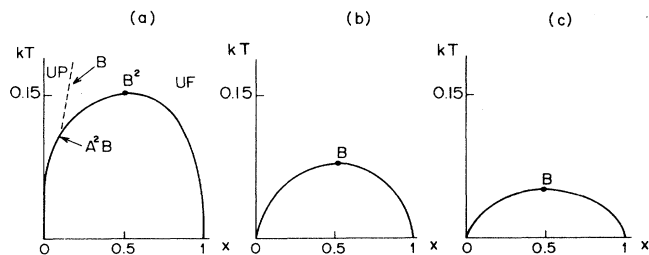


FIG. 7. System phase diagrams for a segregating-ferromagnetic alloy of region 4 in Fig. 1. (a)–(c) as in Fig. 4.

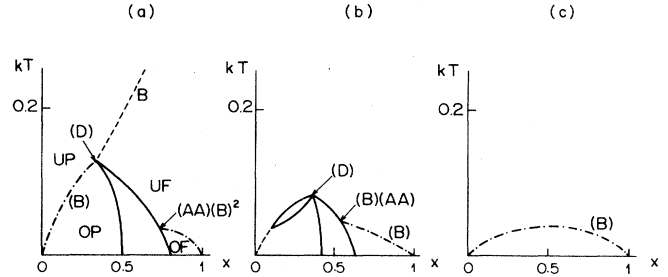


FIG. 8. System phase diagrams for an ordering-ferromagnetic alloy of region 5 in Fig. 1. (a)–(c) as in Fig. 4.

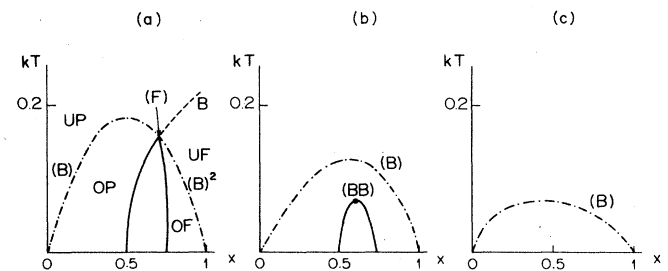


FIG. 9. System phase diagrams for an ordering-ferromagnetic alloy with a value of $c = \frac{1}{2}$ at the boundary of regions 5 and 6 in Fig. 1. (a)–(c) as in Fig. 4.

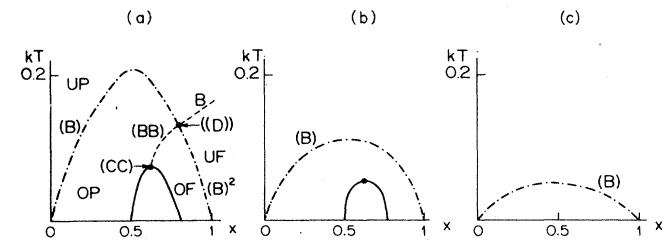


FIG. 10. System phase diagrams for an ordering-ferromagnetic alloy of region 6 in Fig. 1. (a)–(c) as in Fig. 4.

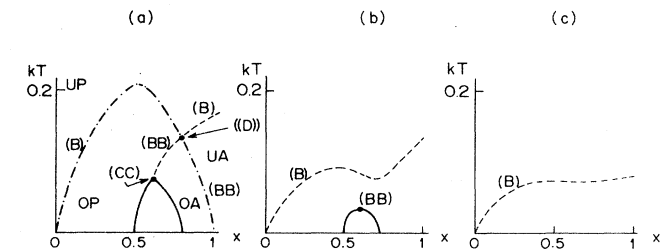


FIG. 11. System phase diagrams for an ordering-antiferromagnetic alloy of region 7 in Figs. 1. (a)–(c) as in Fig. 4.

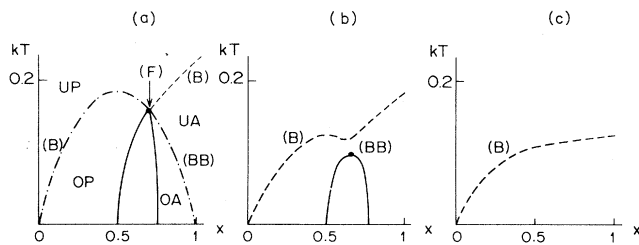


FIG. 12. System phase diagrams for an ordering-antiferromagnetic alloy with a value of $c = -\frac{1}{3}$ at the boundary of regions 7 and 8 in Fig. 1. (a)–(c) as in Fig. 4.

turned on, purely ferromagnetic transitions disappear; however, sublattice-ordered-induced transitions (OF-UF and UP-OP) remain.

In Fig. 8(b) we show a phase diagram for intermediate values of H where a new “lens” of first-order transitions forms via a tricritical point of type (C) along the second-order UP-OP line. For a specific value of H , that chosen for Fig. 8(b), the lens joins the OP-UF transition line via a tetracritical point of type (D). For a larger field, the UP-OP transitions become second order and shift to lower temperatures.

The system phase diagram for the special energy point $c = \frac{1}{2}$ (and $a = -\frac{1}{4}$) displays a sixth-order (F) critical point at zero magnetic field. This multicritical point, shown in Figs. 3 and 9(a), results when the (AA)(B)² critical end point of the OP-OF transitions meets the (D) bound of the UF-OP transitions. It is of interest to note that the structure of the (F) multicritical point is similar to that observed⁶ in CsNiCl₃ where three second-order lines and one of first order merge when a magnetic field is applied to the antiferromagnetic crystal. The intermediate and high-magnetic field diagrams for this energy point are shown in Figs. 9(b) and 9(c), respectively.

As magnetic interactions become weaker in the energy region $\frac{1}{2} > c > 0$, the zero-field OP-OF transitions are only of the first order at low temperatures. These transitions

become second order at a (CC) tricritical point and extend to higher temperatures as (BB) states until they meet the UP-OP dome where they transform at a tetracritical point ((D)) into the B line of UP-UF transitions. This behavior is shown in Fig. 10(a) which, with the exception of the first-order transitions at low temperatures, resembles closely Fig. 2(d) obtained via the simple superposition argument. We note too, from Fig. 3, that the high-order point (F) is also the result of the coalescence of the (CC) and ((D)) states characteristic of this energy region.

C. Ordering antiferromagnetic alloys

$$(-\frac{1}{4} > a > -\frac{1}{2}, -\frac{1}{2} < c < 0)$$

Chemically ordered antiferromagnetic alloys occur when both the heat of mixing $\Lambda = 4a - c$ and the magnetic coupling c are negative; that is, for energy points on the portion of the symmetrical section of the S energy triangle with parameters given by $-\frac{1}{4} > a > -\frac{1}{2}$ and $-\frac{1}{2} < c < 0$. In the absence of an applied magnetic field, the system alloys in this energy interval are antiferromagnetic images [via the mapping shown in Fig. 1] of those systems with energy parameters in the R triangle. The features for the R -triangle section in Fig. 3 are reproduced by the mapping on the image section $-\frac{1}{4} > a > -\frac{1}{2}$ and $-\frac{1}{2} < c < 0$ of the S triangle. The energy point for the system with the (F) state is now located at the center of the S -triangle, and the two regions of different phase behavior that are separated by this special point cover the parameter intervals $(-\frac{1}{3} > a > -\frac{1}{2}, -\frac{1}{3} < c < 0)$ and $(-\frac{1}{4} > a > -\frac{1}{3}, -\frac{1}{2} < c < -\frac{1}{3})$. Notice, too, that the diagrams shown in Figs. 11(a), 12(a), and 13(a) resemble closely those in Figs. 10(a), 9(a), and 8(a), respectively. They differ in the temperatures at which equivalent features occur. Since antiferromagnetic ordering implies sublattice ordering, uniform antiferromagnetic (UA) states correspond to (AA) states in the notation of I and replace the A^2 states of uniform ferromagnetism in triangle R . This implies other changes in the notation (and the nature) of other related states on these diagrams.

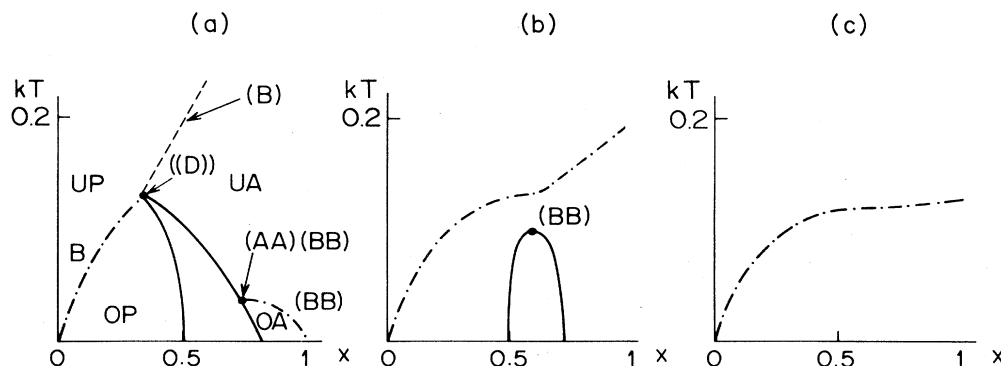


FIG. 13. System phase diagrams for an ordering-antiferromagnetic alloy of region 8 in Fig. 1. (a)–(c) as in Fig. 4.

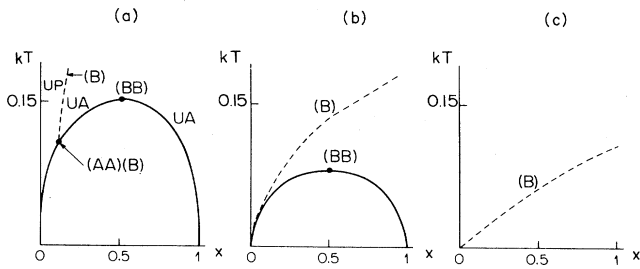


FIG. 14. System phase diagrams for a segregating-antiferromagnetic alloy of region 9 in Fig. 1. (a)–(c) as in Fig. 4.

An applied magnetic field affects the phase properties of ferromagnetic and antiferromagnetic alloys differently. While such a field breaks the twofold degeneracy of ferromagnetic states, it does not do so to that of uniform antiferromagnetic states. Instead, the fourfold degeneracy of ordered antiferromagnetic states is lifted by a nonvanishing field H . A comparison of Figs. 11–13 with Figs. 10, 9, and 8, respectively, shows that when the field is turned on in a ferromagnetic alloy, ordering transitions of chemical origin remain while magnetic transitions are wiped out. The opposite occurs in antiferromagnetic alloys.

D. Segregating antiferromagnetic alloys
 $(0 > a > -\frac{1}{4}, -1 < c < -\frac{1}{2}), \text{ and } (a > 0, c < 0)$

Phase segregation in antiferromagnetic alloys occurs when the heat of mixing $\Lambda = 4a - c > c$ and the magnetic coupling c is negative, that is, for energy points on that portion of the symmetrical section of the S triangle with parameters given by $0 > a > -\frac{1}{4}$ and $-1 < c < -\frac{1}{2}$ and also for energy points on the symmetrical section of the Q triangle, $0 < a < 1$ and $-1 < c < 0$. According to the mapping in Fig. 1, in the absence of an applied magnetic field the system alloys on this energy interval are antiferromagnetic images of the segregating ferromagnetic alloys

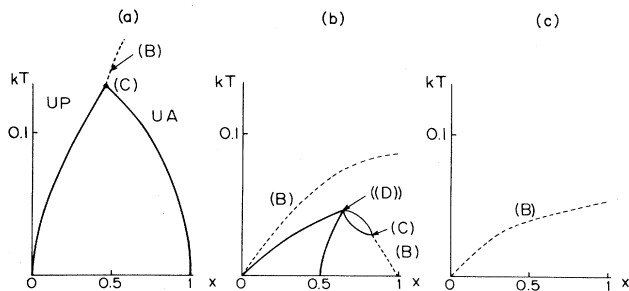


FIG. 15. System phase diagrams for a segregating-antiferromagnetic alloy of region 10 in Fig. 1. (a)–(c) as in Fig. 4.

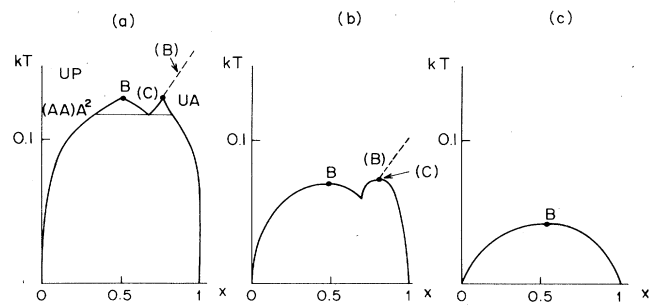


FIG. 16. System phase diagrams for a segregating-antiferromagnetic alloy of region 11 in Fig. 1. (a)–(c) as in Fig. 4.

discussed above. Therefore, all the features shown for the symmetrical section of the P triangle in Fig. 3 are reproduced by the mapping on the image sections on the triangles S and Q . Also, the diagrams shown in Figs. 14(a), 15(a), 16(a), and 17(a) for segregating antiferromagnetic alloys under zero field resemble closely those in Figs. 7(a), 6(a), 5(a), and 4(a), respectively, for their ferromagnetic counterparts. Note the changes in notation for equivalent features between the P , S , and Q sections in Fig. 3 and in the figures mentioned above for the zero-field phase diagrams. These changes reflect the nature of the mapping between ferromagnetic and antiferromagnetic properties described in Sec. II and based on the thermodynamic equivalence of a single sublattice ordered phase with a pair of coexisting uniform phases.⁵

As in the case of ordering alloys, an applied magnetic field affects the phase properties of ferromagnetic and antiferromagnetic segregating alloys differently. A comparison of Figs. 14–17 with Figs. 7, 6, 5, and 4, respectively, shows that when the field is turned on in a ferromagnetic alloy, phase separation is only gradually affected while second-order magnetic transitions are instantly wiped out. In antiferromagnetic alloys, both kinds of transitions persist when H is nonzero. And of these, that which survives last at strong fields depends on the location of the energy point. In Figs. 14 and 15 we show phase diagrams for energy points that represent strong antiferromagnetic interactions, i.e., in the regions $(-\frac{1}{2} < c < -1, -\frac{1}{4} < a < 0)$, and $-1 < c < -0.529$, re-

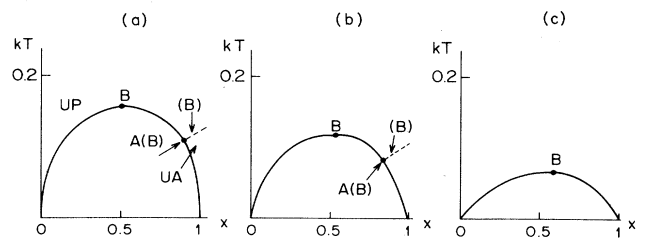


FIG. 17. System phase diagrams for a segregating-antiferromagnetic alloy of region 12 in Fig. 1. (a)–(c) as in Fig. 4.

spectively, the last one on the Q triangle ($a > 0$). Phase segregation dominates over antiferromagnetism. The intermediate-field phase diagrams for energy points that fall within region 10 of Fig. 1, e.g., those shown in Fig. 15(b) are unusually complex and their evolution with increasing H depends on whether the energy point falls on triangle S or Q . [See also the ordering ferromagnet under an applied field shown in Fig. 8(b).]

IV. SUMMARY AND DISCUSSION

Even though magnetic and chemical interactions in solid solutions, their interdependence, and the role they play in determining the phase diagram of alloys have been the subject of extensive theoretical (and to a lesser extent experimental) studies and discussions,^{1,2} a comprehensive and systematic analysis for this problem had not been provided. Here we have taken advantage of the opportunity that the knowledge of the global phase diagram of the FDG three-component model (when both uniform and sublattice-ordered phases are considered) presents for filling this gap within the specific geometry of two interpenetrating sublattices (suitable for simple-cubic and body-centered-cubic lattice systems).

The product of translating the properties of the three-component model into the language of a binary alloy with one magnetic component has been rewarding. We have found a rich variety of phase behavior with many features that had not been previously described for this type of system. Amongst them there are the following. (i) First-order magnetic-to-paramagnetic transitions that take place within chemically ordered phases. This low-temperature behavior is quite general, and it is observed all along the symmetrical sections of triangles R and S that correspond to ordering alloys. (Previous work^{1,7} on

the same model fails in finding this transition and apparently reports one of the associated spinodals as a continuation of second-order transitions). (ii) Phase separation between two magnetically ordered states. [See Figs. 7(a) and 14(a)]. This phenomenon occurs when either ferromagnetic or antiferromagnetic couplings overwhelm the (negative) heat of mixing of the alloy. That is, segregation is driven by magnetic interactions only in a system for which the purely chemical transition corresponds to sublattice ordering. (iii) Three-phase equilibrium between two paramagnetic and one magnetic phases. [See Figs. 5(a) and 16(a).] These states result from the "deadlock" between competing chemical and magnetic interactions that takes place in the so-called shield region^{4,5} on triangle P (and again on its image on triangle Q). (iv) High-order multicritical points. As shown in Fig. 3, and described in the previous section, due to the zero-field degeneracy of uniform and ordered states, there occur different types of bicritical, tricritical, and tetracritical states along the global phase diagram. There are two special alloy systems, one ferromagnetic and the other antiferromagnetic, where a sixth-order critical point occurs. [See Figs. 9(a) and 12(a).] (v) First-order field-induced transitions. [See Fig. 8(b)]. We find this phenomenon in ordering alloys with strong ferromagnetic couplings. Apparently, the second-order UP-OP transition is reinforced by an applied field, which produces different sublattice magnetizations in the ordered phase. Its antiferromagnetic counterpart behaves differently when H is nonzero. [See Fig. 13(b).]

ACKNOWLEDGMENTS

This work was supported in part by Consejo Nacional de Ciencia y Tecnología (CONACyT) de México.

¹G. M. Bell and D. A. Lavis, *Philos. Mag.* **11**, 937 (1965); D. A. Lavis and W. M. Fairbairn, *ibid.* **13**, 477 (1966); D. A. Lavis and G. M. Bell, *ibid.* **15**, 587 (1967).

²M. C. Cadeville and J. L. Morán-Lopez, *Phys. Rep.* **153**, 331 (1987), and references therein. See also M. C. Cadeville and J. L. Morán-Lopez, *Kinam Rev. Fis.* **7c**, 67 (1987).

³C. Varea and A. Robledo, *Phys. Rev. B* **36**, 5561 (1987).

⁴D. Furman, S. Dattagupta, and R. B. Griffiths, *Phys. Rev. B*

15, 441 (1977).

⁵V. Talanquer, C. Varea, and A. Robledo, preceding paper, *Phys. Rev. B* **39**, 7016 (1989) (referred to as I).

⁶M. L. Plumer, K. Hood, and A. Caillé, *Phys. Rev. Lett.* **60**, 45 (1988).

⁷J. L. Morán-Lopez and L. M. Falicov, *J. Phys. C* **13**, 1715 (1980).